NANO LETTERS

LETTER

pubs.acs.org/NanoLett

Coexistence of 1D and Quasi-0D Photoluminescence from Single Silicon Nanowires

Jan Valenta,*,† Benjamin Bruhn,‡ and Jan Linnros‡

†Department of Chemical Physics & Optics, Faculty of Mathematics & Physics, Charles University in Prague, Ke Karlovu 3, 121 16 Prague 2, Czechia

‡Materials Physics, ICT School, Royal Institute of Technology, Electrum 229, 164 40 Kista-Stockholm, Sweden

ABSTRACT: Single silicon nanowires (Si-NWs) prepared by electron-beam lithography and reactive-ion etching are investigated by imaging optical spectroscopy under variable temperatures and laser pumping intensities. Spectral images of individual Si-NWs reveal a large variability of photoluminescence (PL) along a single Si-NW. The weaker broad emission band asymmetrically extended to the high-energy side is interpreted to be due to recombination of quasi-free 1D excitons while the brighter localized emission features (with significantly variable peak position, width, and shape) are due to localization of electron−hole pairs in surface protrusions acting like quasi-0D centers or quantum dots (QDs). Correlated PL and scanning electron microscopy images indicate that the efficiently emitting QDs are located at the Si-NW interface with completely oxidized neck of the initial Si wall. Theoretical fitting of the delocalized PL emission band explains its broad asymmetrical band to be due to the Gaussian size distribution of the Si-NW diameter and reveals also the presence of recombination from the Si-NW excited state which can facilitate a fast capture of excitons into QD centers.

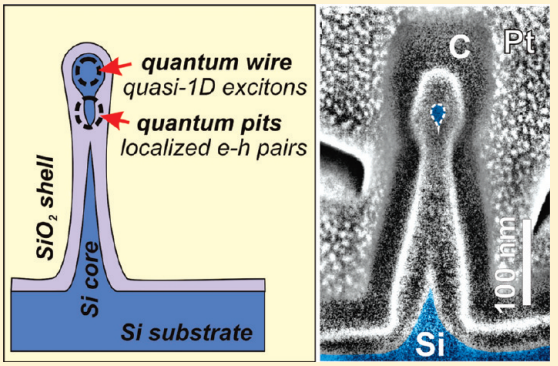

KEYWORDS: Nanowire, quantum dot, silicon, luminescence, exciton

Light-emitting properties of Si nanowires (Si-NWs) are relatively little explored compared to silicon quantum wells (quasi-2D structures) and, especially, quantum dots (quasi-0D structures).[1] However, the interest in understanding electron−hole generation and recombination in silicon nanowires has been rapidly growing during the last years when new methods of Si-NW mass production have been introduced.[2,3] Their potential applications include mainly novel solar cells,[4−6] detectors and sensors,[7] battery electrodes,[8] etc. Regardless of the fabrication technique, luminescence characterization of grown Si-NWs is potentially the most convenient (fast, nondestructive, and sensitive) characterization technique if properly understood and related to structural information.

Photoluminescence (PL) of Si-NWs was addressed by several groups with results very similar to other Si-based nanostructures (porous and nanocrystalline Si). Namely observing broad PL spectra in the orange−red−near-IR spectral region[9,10] and sometimes also blue emission[11] which is often ascribed to defects in the SiO_2 shell.[12] As the most interesting observations, we can highlight the increase of absorption cross section, the suppression of Auger recombination (Auger lifetime was found to be about 2 orders of magnitude longer compare to Si nanocrystals),[13] and the very high (nearly complete) linear polarization ratio of PL from Si-NWs.[14] The inevitable variations of Si-NW diameter create potential traps that can act as localization centers for electron−hole pairs. However, the related question on the role of delocalized 1D excitons and localized quasi-0D excitons in the photoluminescence emission from Si-NWs was not resolved up to now.

In this paper we demonstrate localized emission from 0D-like quantum dot centers as well as emission from delocalized 1D-like excitons. Both types of emission originate from the same structures, i.e. from nanowires made of oxidized silicon walls. The walls have been fabricated from silicon wafers using electron-beam lithography, plasma etching, and by careful oxidation in the self-limiting oxidation regime.[15] The distinction between the two types of recombination becomes possible as the quantum dot emission is characterized by a local emission center (in the emission image captured by a CCD camera) and by a relatively sharp luminescence peak. The 1D exciton emission on the other hand is distributed along a single nanowire and is characterized by a broad spectrum starting at a lower energy. The broad spectrum most likely comes from thickness variation and a corresponding confinement energy variation along the nanowire. Excitons may possibly transfer from the 0D centers to 1D nanowires in our structures, or vice versa. This would require more dedicated experiments and in this paper the main point remains to prove the coexistence of the two different excitons.

The Si-NW fabrication procedure is similar to the one described in a previous paper.[16] Negative resist HSQ was spun onto n-type (20 Ω·cm resistivity) 10 × 10 mm^2 Si(100) wafer

Received: May 13, 2011
Published: June 28, 2011

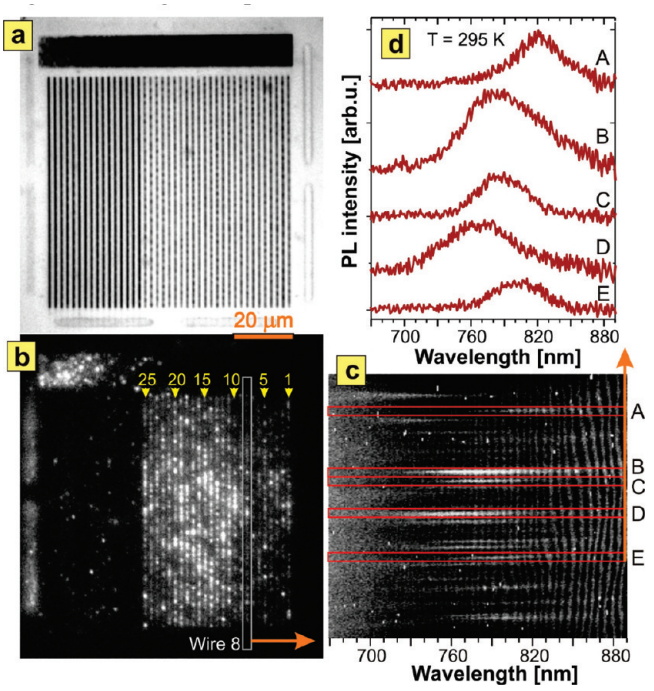

Figure 1. The principle of single Si-NW measurement (T = 295 K): (a) reflection and (b) photoluminescence image of a part of a group of Si-NWs (distance between adjacent wires is 2 μm and long bright wires are numbered from right to left, see yellow numbers and arrows). The NW-8 is selected (gray rectangle in (b)) and its spectral image (c) is detected. The spectral traces of five intensely emitting spots are selected (red rectangles labeled A to E) and their spectra plotted in (d).

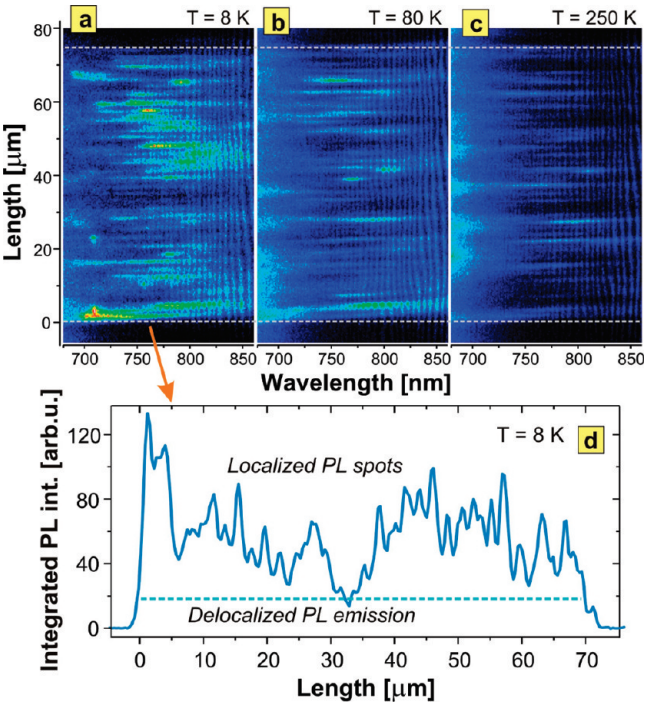

Figure 2. PL spectral traces for the NW-19 taken at (a) 8, (b) 80, and (c) 250 K. Hot spots were removed from these images (in contrast to Figure 1c). The horizontal dashed lines indicate extremes of the wire. The panel (d) reveals the intensity profile of integrated PL signal (from 680 to 860 nm) at 8 K (it means sum of PL signal from panel a along the vertical lines). Delocalized PL emission along the whole wire is seen as the continuous background signal which exceeds the signal outside the wire.

pieces at 6000 rpm and baked for 10 min at 150 °C. Line patterns were exposed using electron beam lithography (EBL), and the sample was developed in a MF-CD26 bath (1 min). HBr-based reactive ion etching (RIE) transferred the patterns into the bulk silicon, resulting in standing silicon walls. These were then oxidized for 30 min at 900 °C, which led to nanowire formation in the top of the wall. Si-NWs are oriented along the [100] direction.

The sample morphology was visualized using a Zeiss Gemini scanning electron microscope (SEM) at 20 kV acceleration voltage, which enables a distinction between remaining silicon core and oxidized parts of the walls. Cross sections of the oxidized silicon walls were performed with a FEI Nova 200 focused ion beam (FIB) after deposition of first a carbon layer and then a platinum protection layer.

Figure 1 shows reflected (a) and PL (b) microimages of part of the lithography-defined structure, which contains 25 efficiently emitting Si-NWs (about 74 μm long). These Si-NWs were used to obtain the results presented in this paper. They are numbered starting from the right side, as indicated in Figure 1b.

Photoluminescence microspectroscopy was performed using a home-built setup based on an inverted microscope coupled to a 30 cm imaging spectrograph with a back-thinned CCD camera. Samples were mounted on a special copper holder in a coldfinger of a cryostat (available temperature range is about 5−300 K). A single objective lens (40×/0.6 with correction for influence of a cryostat window) was used to focus excitation light as well as collect and image emitted signal (epifluorescence configuration). Excitation by the 405 nm diode laser was sent to a sample through an optical system which allowed exciting a wide field of a sample (approximately 32 μm in diameter). The excitation power density was variable between ~0.04 and 80 W/cm^2 using neutral density filters. Alternatively to the excitation laser, white halogen lamp light can be sent to the sample in order to observe reflection images of the studied structures. Silicon nanowires were oriented parallel to the spectrometer entrance slit (and parallel to the polarization of the laser excitation as the excitation efficiency is strongly polarization dependent[17]). Then the entrance slit was closed to ~0.13 mm in order to image just one single Si-NW and detect its spectral image (see Figure 1). The resolution of the different emission spots within an individual Si-NW is given by the diffraction limit to about 800 nm. Typical acquisition times for low-temperature spectral microimages are between 30 and 60 min, therefore the position drift of a sample in a cryostat must be less than 1 μm/h. All spectra were corrected to the spectral response of the apparatus. In the infrared part of the detected range (see, e.g., Figures 1c and 2a−c) the back-thinned CCD chip exhibits a strong etaloning effect. It can be corrected by appropriate correction curves and additionally by the adjacent-points averaging. Also hot spots (see Figure 1c) are usually corrected (by replacing with neighbor pixel signal value) in the presented spectra.

The advantage of imaging spectroscopy of single Si-NWs is that the luminescence spectra variations along an individual NW are directly visualized. In Figure 2 we present three such snapshots showing spectral images of Si-NW no. 19 (see numbers in Figure 1b) at three different temperatures. One can make several observations which are generally valid for all measured Si-NWs: (i) There is a weak quasi-continuous delocalized emission along

dx.doi.org/10.1021/nl201610g |*Nano Lett.* 2011, 11, 3003–3009

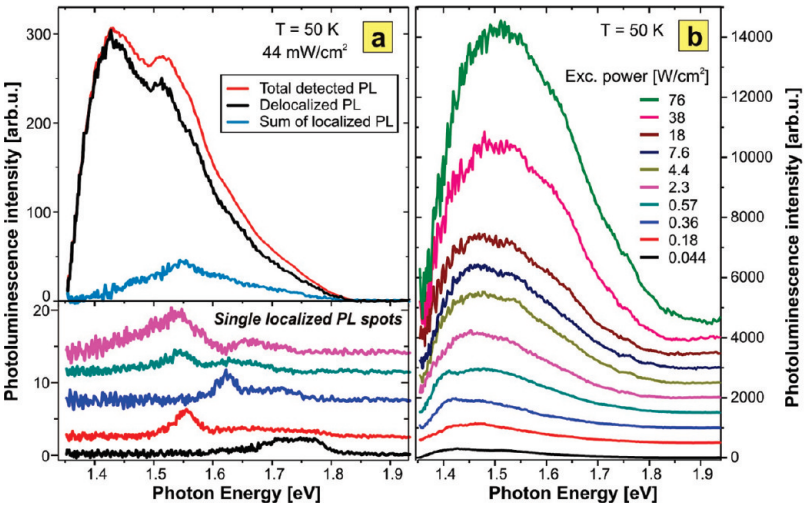

Figure 3. Characteristics of the delocalized PL emission of NW-19 at $T = 50$ K: (a) Total integrated PL signal (red line), the sum of localized PL spectra (blue line) and their difference (black line) taken at the lowest excitation density of 44 mW/cm^2. Five typical single spot PL spectra are shown below with expanded intensity scale. (b) Excitation intensity dependence of the integrated PL spectra of NW-19 (localized PL emission is subtracted).

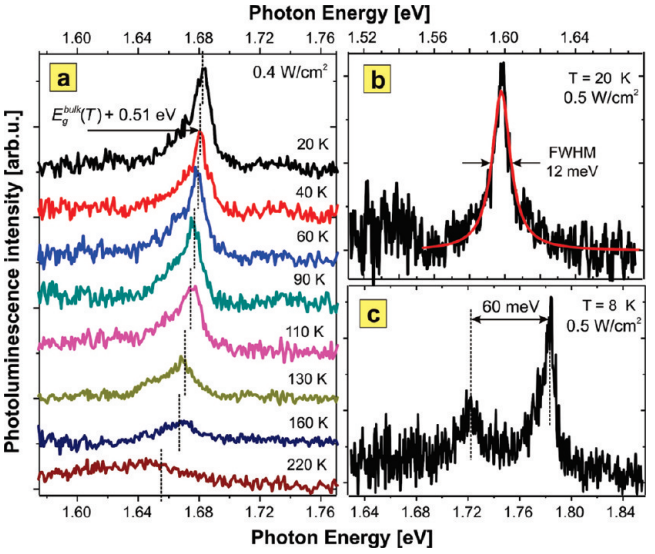

Figure 4. Single-quantum-dot-like PL spectra from localized spots in Si-NWs. (a) The temperature dependence of one localized emission peak—the peak position follows the thermal shift of Si band gap (eq 1) with constant confinement energy of 0.51 eV. The emission disappears around 220 K. (b) The Lorentzian fit of one narrow emission spot with fwhm of 12 meV (the k_BT energy at $T = 20$ K is about 1.7 meV). (d) Another localized PL spectrum with well-pronounced TO-phonon sideband shifted by 60 meV below the main (zero-phonon) peak.

the whole NW which exceeds the background signal (outside a NW), especially at low temperatures (see Figure 2d where integrated PL intensity profile obtained from Figure 2a is presented). (ii) A few points in the NW have much stronger emission than the continuous signal and their spectral position and shape (number and width of emission bands) is strongly variable, (iii) these intense spectra are less abundant and somehow wider at higher temperatures (compare panels a−c in Figure 2).

In Figure 3a we compare different components of the NW-19 PL signal at $T = 50$ K. The red line represents the overall integrated and corrected PL spectrum (the adjacent averaging was applied to smooth the spectrum), the blue line is the sum of all distinguishable localized PL spot spectra (five of these localized spectra are shown in the bottom part of Figure 3a with expanded intensity scale), and the black line is the difference of the overall and localized spectra. It is clear that the continuous emission exceeds the sum of localized emission by an order of magnitude (at this temperature of 50 K) even if its brightness (intensity per unit area) is lower. When we "clean" the delocalized emission spectrum from the localized one (black line) the shape has a form of a wide band with a tail extended to the high-energy side. Under increasing excitation power density the emission peak is shifting to higher energy and its width becomes broader (Figure 3b).

The bright localized emission is characterized by two generally valid observations. First, the localized emission spectra are always at photon energies higher than the observed continuous emission peak starting at 1.43 eV. The second observation is the extreme variability of the emission spectral width, shape, and peak position. The obvious origin of the variable position can be the size-dependent energy level shift (quantum confinement) and the variable width could be due to unresolved inhomogenous broadening (several emitting centers within the optically resolved emission spot, we remind that the spatial resolution of our microscopic imaging of the sample inside the cryostat is about 800 nm). Although inhomogeneous broadening cannot be completely excluded, we suppose that the main origin of the variable emission bandwidth is a *variation of the electron−hole pair localization strength* as will be explained below.

The localized emission spectra often closely resemble the spectra of individual Si nanocrystals (quantum dots) reported in the literature. They can be very narrow (Figure 4a,b) and often reveal a TO-phonon replica at 60 meV (Figure 4c) in analogy to low-temperature PL spectra of individual Si quantum dots reported by Sychugov et al.[18] The PL peaks are slightly shifting to lower energies with increasing temperature (Figure 4a) which is in perfect agreement with the shrinking of the Si band gap described by the equation[19]

$$E_g^{bulk}(T) = 1.170 - \frac{(4.73 \times 10^{-4})T^2}{636 + T} \qquad (1)$$

dx.doi.org/10.1021/nl201610g |*Nano Lett.* 2011, 11, 3003–3009

Along with the red shift, the localized PL intensity is quenched with increasing T, fastest rate being between 120 and 180 K. The temperature dependence of the integrated intensity of single localized PL emissions (Figure 5a) reveals an Arrhenius-type quenching,[20] which is fitted using the equation

$$I(T) = \frac{I_0}{1 + C\ exp(-E_a/kT)} \quad (2)$$

The activation energy E_a is typically ~70 meV but varies from dot to dot and sometimes is high enough to observe PL even at room temperature. As an example, the integrated signal of PL peaks from Figure 4a is plotted in Figure 5a (blue dots and dashed line) revealing an activation energy of 78 meV. We have to note that a similar temperature quenching activation energy (around 70 meV) was observed also in porous Si.[20] On the other hand the temperature dependence of the integrated continuous PL signal (black squares in Figure 5a) shows a stronger quenching with an activation energy of E_a = 25 meV.

In Figure 5b we plot the pumping power intensity dependence of the integrated PL signal of the delocalized emission (black squares) and the summed localized spot signals (blue circles, NW-19 at 50 K, data from Figure 3). Even if such data are subject of significant fluctuations (collection of the full intensity dependence takes many hours, demanding perfect stability of the experimental system), it can provide a hint about the importance of Auger recombination. The localized emission often reveals excitation power dependence with a saturation characterized by the power-law dependence with an exponent close to 2/3. This saturated intensity exponent seems to be a very general feature for Si nanocrystals. For example, Valenta et al. reported the intensity dependence of PL from single Si nanocrystals (excluding the ON/OFF blinking effect) following an $I_{exc}^{0.7}$ dependence (which is virtually equal to 2/3 slope within statistical error).[21] In the literature, this kind of intensity dependence was explained as a combination of "classical" three-particle Auger recombination (responsible for $I_{exc}^{1/3}$) and bimolecular recombination[22,23] or biexciton-like recombination (responsible for an I_{exc}^{2} dependence).[24] On the other hand, the integrated delocalized spectral intensity (taken from Figure 3b) increases with pumping intensity approximately as the square root. It indicates excitonic character of emission which is limited by *bimolecular Auger recombination* (in fact a kind of inelastic exciton−exciton scattering leading to nonradiative recombination of one and excitation of the second exciton) when overcoming a certain pumping threshold. It is supposed to correspond to a situation when the mean distance of excitons is about to be equal to the exciton Bohr radius, thus it depends on exciton lifetime—at low temperatures exciton lifetime in Si structures becomes considerably long (>0.1 ms) and within the available range of pumping density the system is already in the Auger limited regime. To resume the PL power dependence, it indicates importance of Auger recombination which limits the population of electron−hole pairs (excitons) above a certain pumping threshold but it does not quench the PL signal completely (at least for pumping powers exceeding the Auger threshold by 2 orders of magnitude).

In order to correlate the observed local variations of PL with morphological changes, we investigated Si-NWs with a scanning electron microscope operated at high voltage, which is able to distinguish between Si and SiO_2 (Figure 6). A series of images taken at 150000× magnification can be combined to a complete high resolution image of the whole 74-μm-long silicon wall (Figure 7a). These measurements were performed after the PL measurements in order to avoid electron-beam induced crystal lattice damage.

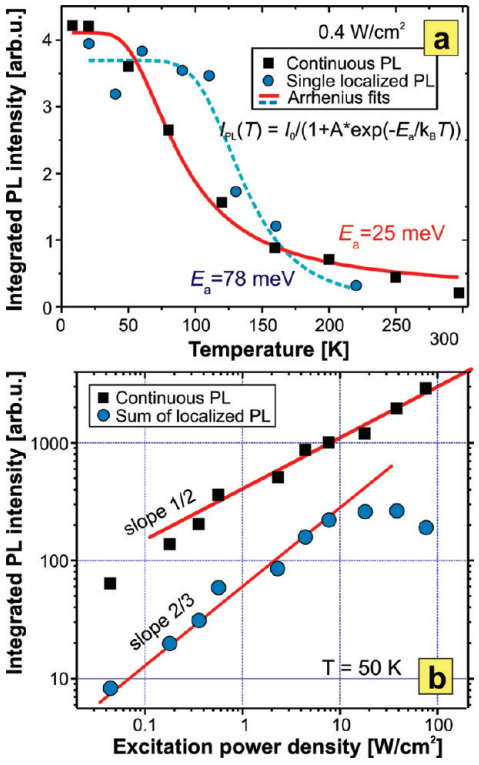

Figure 5. (a) Temperature dependence of the integrated continuous PL signal of NW-19 (black squares) and an example of localized PL emission (blue dots) for spectra plotted in Figure 4a). The T-dependences are fitted by an Arrhenius thermally activated PL decay curve (eq 2); the corresponding activation energies are indicated. (b) The excitation power dependence of the integrated PL signal of NW-19. The continuous PL emission (black squares) and sum of localized emission (blue circles) are compared with the power dependence having exponents 1/2 and 2/3 (red lines), respectively.

As already demonstrated in a previous paper,[25] Si NW formation takes place in the upper part of the Si walls due to self-limiting oxidation. Even if the center of the wall is not fully oxidized (white parts in Figure 6), it is the narrowest part of the wall with the strongest confinement and the widest band gap acting as a barrier which keeps excitons in the upper part of the wall (nanowire). Full oxidation of the wall neck (dark parts in Figure 6) leads to the observation of strong local PL spots. In these parts the silicon core (NW) edge is not smooth, but contains random protrusions. Figure 7a demonstrates the rough correlation of the PL signal maxima with dark areas in the SEM images of the same wire (or, vice versa, the correlation of PL minima with white—not fully oxidized—parts). The SEM image is combined from a series of snapshots taken along the wire with a period of about 1.7 μm (the overlapping areas appear darker).

In view of the presented PL and SEM experiments on single Si nanowires, we can interpret the delocalized PL emission, characterized by a broad spectrum, to be due to radiative recombination of 1D excitons confined in the upper part of the oxidized Si walls. This weak emission is observed in all Si-NWs which are separated from the substrate either by a narrow Si neck or even by

dx.doi.org/10.1021/nl201610g |*Nano Lett.* 2011, 11, 3003–3009

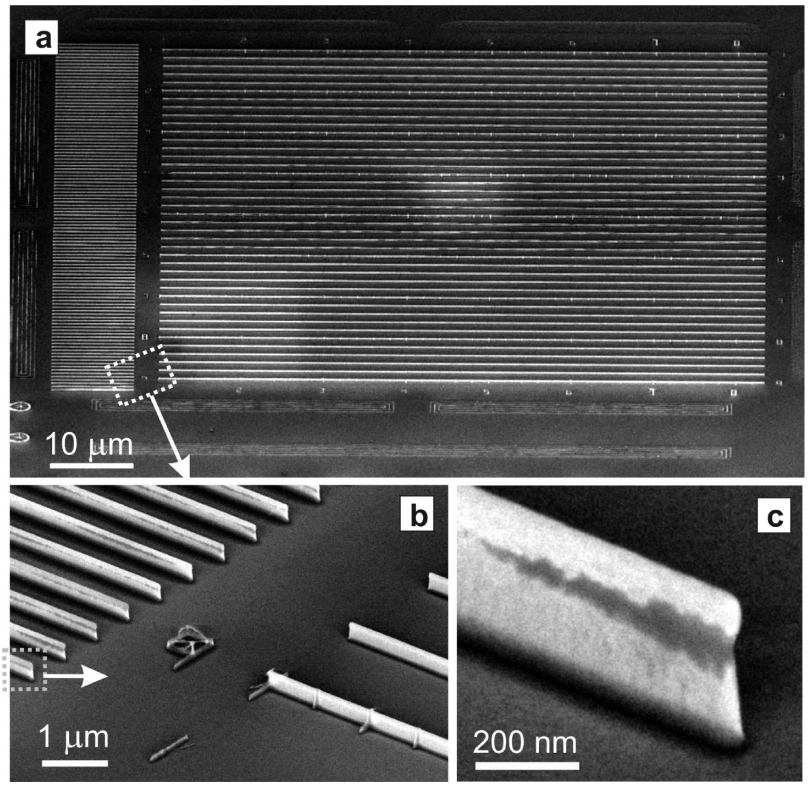

Figure 6. SEM imaging: (a) The overall SEM image of the area whose optical reflection and PL images are shown in Figure 1a,b (the SEM image is rotated 90° counterclockwise related to optical images). (b) A detail of small part of structure (indicated by white dashed rectangle in panel a) where the more densely spaced walls on the left-hand side reveal black spots in the wall neck indicating complete oxidation. This part of sample has strong PL brightness while the wires on the right-hand side shows no strong PL spots and their neck is not oxidized through. (c) The SEM detail of one wire end whose neck is oxidized through and random extrusions are seen on the lower interface of a wire with an oxidized neck.

a completely oxidized neck. On the other hand the brighter localized PL emission with strongly variable spectral position and shape is observed only in Si walls that contain parts of completely oxidized wall necks. These dots display all characteristics of single quantum dots such as blinking, narrow emission band, individual peak energies (most likely due to size dispersion), and phonon replicas. The SEM images correlated with PL profiles suggest that the generated electron−hole pairs can be localized in protrusions randomly generated at the interface between a Si-NW and the completely oxidized neck of a Si wall (see Figure 6c). Localization of excitons in the points where a Si-NW is locally broader can be excluded as such a local quantum well has smaller confinement, narrower band gap, and consequently a PL shifted to lower energy, which is inconsistent with the observed localized PL shifted to higher energy from the 1D emission peak.

So we propose that the localized centers have a form of defect traps, e.g. surface protrusions on the lower nanowire interface (named "quantum pits", Figure 7b), where e−h pairs are localized (with variable localization strength, having variable shape between "pure" 1D exciton and 0D quantum dot exciton) and recombine in a way similar to bound excitons in bulk crystals. Actually, such trapping centers were theoretically described by Cantele et al.[26] They have shown that on the surface of a deformed quantum wire a very rich surface electronic structure comes out from the surface topology and calculated localization energies of up to 0.2 eV and possibly higher for bigger defects. A similar conclusion on the important role of surface "bulbs" in PL of Si-NWs was recently proposed by Sivakov et al. who correlated high-resolution TEM of SiNWs with their ensemble PL measurements.[27] The localization effects can also explain relatively weak size dependence of PL peak position reported by Guichard et al.[9] Another theoretical study by Wang et al.[28] supports our interpretation by showing that the formation of trapped excitons is likewise for short Si nanorods only, while longer wires exhibit fully delocalized excitons with negligible geometrical distortion at the excited state minimum.

Let us now address the question why the shape of the delocalized emission is so broad and asymmetrically extended to the high energy side. At first sight this spectral shape can resemble the $E^{-1/2}$ form of the density of states (DOS) in 1D semiconductor structures.[29] However, this cannot be the source of the asymmetrical shape here as the fwhm of the observed PL band is more than 0.2 eV while the fwhm of the 1D "free" excitonic emission line (combining the 1D DOS and exponentially decaying Maxwell−Boltzmann distribution[30]) should be less than k_BT (i.e., 4.3 meV at 50 K and 26 meV at 300 K). In our opinion, the only effect, which can produce such broad PL spectrum, is an inhomogeneous broadening due to the variation of Si-NW diameter. In order to explore this possibility, we try to fit the spectral shape with a model Si-NW size distribution (and assuming that each size of Si-NW within this distribution produces PL with equal efficiency). In literature, one can find very heterogeneous theoretical relations between the Si-NW diameter and its PL peak position,[31,32] but most of them have the form of $E_{peak} = E_g^{bulk} + Cd^{-\alpha}$, where α is equal to 2 for the simplest effective mass approximation, but is closer to 1 for more realistic models. Here we adopt the relation for quasi-

dx.doi.org/10.1021/nl201610g |Nano Lett. 2011, 11, 3003–3009

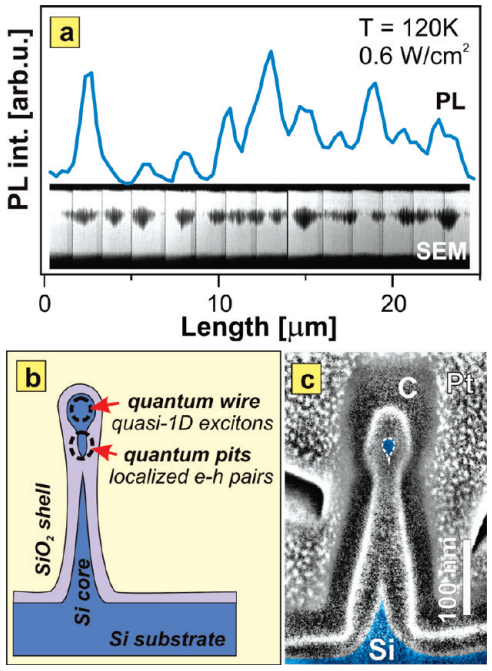

Figure 7. (a) A part of NW-19 documenting the spatial correlation of integrated PL signal intensity with location of oxidized wall neck visualized by sequential SEM images. (b) Schematical sketch of a Si-NW cross section and position of nanowire and localized quantum pits within a NW. (c) SEM image of an oxidized Si wall cross section made with a focused ion beam. The structure was covered by carbon and platinum layers prior to cutting. The image was numerically enhanced by the local equalization treatment and the silicon part was blue-colored. Approximate dimensions of a Si-NW in the top part of the Si wall is 16 × 22 nm in horizontal and vertical directions, respectively.

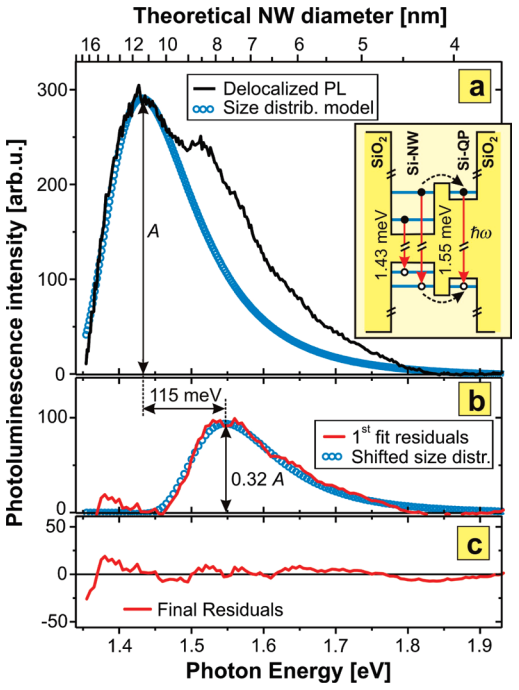

Figure 8. Modeling the delocalized PL spectrum of NW-19 (T = 50 K) with a symmetrical Gaussian distribution of Si-NW diameters transformed to the PL peak energy using the theoretical relation given by eq 3 (it was also used to calculate the upper scale of theoretical size of NWs): (a) Theoretical fit corresponding to Gaussian distribution with center at 11.4 nm and fwhm of 6.0 nm (light blue circles). (b) Residuals from the above given fit are again fitted by the same Gaussian distribution shifted by 115 meV and lowered 3.2 times (cyan circles). (c) The final residuals after the two fits. The inset in panel a illustrates the two observed states of Si-NW and their possible relation to the localized QP states.

particles (QP) band gap in a Si-NW derived by Bruno et al.[33] by applying DFT-LDA (density functional theory and local density approximation) methods. By fitting their points calculated for Si-NWs grown along the [100] direction, we obtained the quasiparticle band gap (without excitonic effects) described by

$$E_{\text{peak}}\ (\text{eV}) = 1.16\ (\text{eV}) + 2.49\ (\text{eV/nm})\ d^{-0.91}\ (\text{nm}) \quad (3)$$

Then if we suppose that the Si-NW diameter distribution is symmetrical, eq 3 transforms it into an asymmetrical PL peak distribution. We searched for a symmetrical Gaussian distribution of Si-NW diameters which will fit the observed PL peak shape as closely as possible. The result is shown in Figure 8a by the blue empty circles—the central diameter and the fwhm of the Gaussian band are 11.4 and 6.0 nm, respectively. This roughly corresponds to the estimated size of the Si-NW core at the top of the Si wall revealed by SEM imaging of a Si wall cross section, obtained by focused-ion-beam cutting (Figure 7c). The calculated distribution fits very well the low energy side of the spectrum but leaves a part of the PL intensity around 1.54 eV. Surprisingly, the residual between the PL spectrum and the fitted function has again an asymmetrical shape (Figure 8b) and can be perfectly fitted with the same size distribution just shifted by 115 meV and its amplitude decreased 3.2 times. The final residual (Figure 8c) is close to zero. So, we have clearly two inhomogeneously broadened emitting states. Under stronger pumping (Figure 3b) the high-energy peak disappears and the whole spectrum becomes broader and blue-shifted. This effect is probably due to phase space filling—stronger pumping increases the density of excitons that are forced by the Pauli principle to occupy higher lateral quantization subbands of the NW.[34]

We propose that the high energy state is an excited state of the 1D quantum well (see the inset in Figure 8a). Because its peak at 1.545 eV is close to the most abundant PL peak of localized centers (Figure 3a), we can expect that the efficiency of exciton trapping in quantum dots may be resonantly enhanced. However, recall that both NW and QD levels are broadly distributed so many local arrangements of Si-NW and QD levels are possible.

We have to note that our Si-NWs with surface protrusion can be considered as a model material explaining the rich PL properties of electrochemically etched Si structures known as porous silicon, which are still not fully understood after more than 2 decades of intensive investigation.[1] The coexistence of 1D and 0D PL emissions can also explain troubles with theoretical modeling of the PL size dependence in porous Si and some Si nanowire structures.[27]

In conclusion, we have performed photoluminescence measurements of single Si nanowires prepared by electron-beam lithography, plasma etching and oxidation. The overall emission of a Si-NW and localized bright emission from spots within a Si-NW is resolved and studied for many individual NWs under temperatures between 8 and 300 K and excitation densities from 0.04 to 80 W/cm^2. The delocalized PL with a broad PL spectrum is interpreted as recombination of 1D excitons in Si-NWs formed at the top of Si walls. On the other hand stronger localized PL with variable spectral shapes is found only in locations where the lower interface between a Si-NW and the completely oxidized neck of a Si wall

dx.doi.org/10.1021/nl201610g |Nano Lett. 2011, 11, 3003–3009

contains irregular extrusions, which most probably act as traps (quantum pits) where electron−hole pairs are localized and produces emission similar to quasi-0D quantum dots. Our interpretation of luminescence properties of individual Si-NWs may be applied to understand the extremely variable optical properties of porous Si and other Si nanostructures. The practical consequences of coexistence of 1D and 0D effects in Si-NWs can be multiple: (i) an optimization of the density and shapes of localized centers should significantly increase the brightness (and reduce saturation effects) of Si-NW PL, especially at room temperature; (ii) after a more detailed understanding of the relation between the local structure and PL spectra, the micro-PL spectral imaging may be applied to detailed characterization of fabricated Si-NWs; (iii) the coexistence of delocalized and localized centers is also crucial for application of Si-NW as sensors and detectors.

AUTHOR INFORMATION

Corresponding Author

*E-mail: jan.valenta@mff.cuni.cz.

ACKNOWLEDGMENT

The authors thank Professor I. Pelant and Professor S. Ossicini for discussions. Financial support from the Swedish Research Council (VR) through an individual and a Linné grant is gratefully acknowledged. Part of this work (J.V.) was supported through the research centre LC510 and the research plan MSM0021620835 of MSMT and the project KAN400100701 of the GAAV.

REFERENCES

(1) *Silicon nanocrystals: Fundamentals, Synthesis and Applications*; Pavesi, L., Turan, R., Eds.; Wiley-VCh: Weinheim, 2010.
(2) Schmidt, V.; Wittemann, J. V.; Gösele, U. *Chem. Rev.* **2010**, *110*, 361–388.
(3) Bandaru, P. R.; Pichanusakorn, P. *Semicond. Sci. Technol.* **2010**, *25*, 024003.
(4) Kelzenberg, M. D.; Turner-Evans, D. B.; Kayes, B. M.; Filler, M. A.; Putnam, M. C.; Lewis, N. S.; Atwater, H. A. *Nano Lett.* **2008**, *8*, 710–714.
(5) Sivakov, V.; Andra, G.; Gawlik, A.; Berger, A.; Plentz, J.; Falk, F.; Christiansen, S. H. *Nano Lett.* **2009**, *9*, 1549–1554.
(6) Kelzenberg, M. D.; Boettcher, S. W.; Petykiewicz, J. A.; Turner-Evans, D. B.; Putnam, M. C.; Warren, E. L.; Spurgeon, J. M.; Briggs, R. M.; Lewis, N. S.; Atwater, H. A. *Nat. Mater.* **2010**, *9*, 239–244.
(7) Agarwal, A.; Buddharaju, K.; Lao, I. K.; Singh, N.; Balasubramanian, N.; Kwong, D. L. *Sens. Actuators, A* **2008**, *145*, 207–213.
(8) Chan, C. K.; Peng, H.; Liu, G.; McIlwrath, K.; Zhang, X. F.; Huggins, R. A.; Cui, Y. *Nat. Nanotechnol.* **2008**, *3*, 31–35.
(9) Guichard, A. R.; Barsic, D. N.; Sharma, S.; Kamins, T. I.; Brongersma, M. L. *Nano Lett.* **2006**, *6*, 2140–2144.
(10) Walavalkar, S. S.; Hofmann, C. E.; Homyk, A. P.; Henry, M. D.; Atwater, H. A.; Scherer, A. *Nano Lett.* **2010**, *10*, 4423–4428.
(11) Qi, J.; Belcher, A. M.; White, J. M. *Appl. Phys. Lett.* **2003**, *82*, 2616–2618.
(12) Dovrat, M.; Arad, N.; Zhang, X. H.; Lee, S. T.; Sa'ar, A. *Phys. Status Solidi A* **2007**, *204*, 1512–1517.
(13) Guichard, A. R.; Kekatpure, R. D.; Brongersma, M. L. *Phys. Rev. B* **2006**, *78*, 235422.
(14) Ma, D. D. D.; Lee, S. T.; Shinar, J. *Appl. Phys. Lett.* **2005**, *87*, 033107.
(15) Liu, H. I.; Biegelsen, D. K.; Ponce, F. A.; Johnson, N. M.; Pease, R. F. W. *Appl. Phys. Lett.* **1993**, *64*, 1383–1385.
(16) Bruhn, B.; Sangghaleh, F.; Linnros, J. *Phys. Status Solidi A* **2011**, *208*, 631–634.
(17) Valenta, J.; Bruhn, B.; Linnros, J. *Phys. Status Solidi C* **2011**, *8*, 1017–1020.
(18) Sychugov, I.; Juhasz, R.; Valenta, J.; Linnros, J. *Phys. Rev. Lett.* **2005**, *94*, 087405.
(19) Sze, S. M. *Physics of Semiconductor Devices*, 2nd ed., Wiley InterScience, New York, 1981.
(20) Andersen, O. K.; Veje, E. *Phys. Rev. B* **1996**, *53*, 15643–15652.
(21) Valenta, J.; Fucikova, A.; Vacha, F.; Adamec, F.; Humpolíčková, J.; Hof, M.; Pelant, I.; Kůsová, K.; Dohnalová, K.; Linnros, J. *Adv. Funct. Mater.* **2008**, *18*, 2666–2672.
(22) M'ghaïeth, R.; Maâref, H.; Mihalcescu, I.; Vial, J. C. *Phys. Rev. B* **1999**, *60*, 4450–4453.
(23) Tayagaki, T.; Fukatsu, S.; Kanemitsu, Y. *Phys. Rev. B* **2009**, *79*, 041301.
(24) Dal Negro, L. *PhD thesis*, Università di Trento, 2003.
(25) Bruhn, B.; Valenta, J.; Linnros, J. *Nanotechnology* **2009**, *20*, 505301.
(26) Cantele, G.; Ninno, D.; Iadonisi, G. *Phys. Rev. B* **2002**, *61*, 13730–13736.
(27) Sivakov, V. A.; Voigt, F.; Berger, A.; Bauer, G.; Christiansen, S. H. *Phys. Rev. B* **2010**, *82*, 125446.
(28) Wang, Y.; Zhang, R.; Frauenheim, T.; Niehaus, T. A. *J. Phys. Chem. C* **2009**, *119*, 12935.
(29) Dawies, J. H. *The physics of low-dimensional semiconductors: An introduction*; Cambridge University Press: Cambridge and New York, 1998.
(30) Peyghambarian, N.; Koch, S. W.; Mysyrowicz, A. *Introduction to Semiconductor Optics*; Prentice Hall: Englewood Cliffs, NJ, 1993.
(31) Li, J.; Freeman, A. J. *Phys. Rev. B* **2006**, *74*, 075333.
(32) Yao, D.; Zhang, G.; Li, B. *Nano Lett.* **2008**, *8*, 4557–4561.
(33) Bruno, M.; Palummo, M.; Marini, A.; Del Sole, R.; Ossicini, S. *Phys. Rev. Lett.* **2007**, *98*, 036807.
(34) Forchel, A.; Kieseling, F.; Braun, W.; Ils, P.; Wang, K. H. *Phys. Status Solidi B* **1995**, *188*, 229–240.